Pergamon

*Int. J. Heat Mass Transfer.* Vol. 39, No. 18, pp. 3899–3910, 1996

0017–9310/96 $15.00 + 0.00

PII: S0017–9310(96)00054–3

# Scaling of boundary-layer flows driven by double-diffusive convection

A. MONGRUEL, M. CLOITRE and C. ALLAIN

Laboratoire Fluides, Automatique et Systèmes Thermiques, Bâtiment 502, Campus Universitaire, 91405 Orsay Cedex, France

(*Received* 23 *December* 1994 *and in final form* 12 *January* 1996)

**Abstract**—The objective of this paper is to investigate natural convection driven by two buoyancy sources, such as heat and mass, in vertical boundary layers. Starting from the integral equations and using scale analysis, we derive the different asymptotic flow regimes encountered with different buoyancy forces and diffusion coefficients. Each type of flow is characterized by a set of scaling relations yielding the velocity, temperature and concentration distributions inside the fluid, and the heat and mass transfer coefficients. All our results are perfectly corroborated by numerical investigations in a wide range of parameters.


## 1. INTRODUCTION

Double-diffusive convection takes place in fluids where two components with different diffusivities (heat, solute concentration or phase compositions) act in conjunction to create buoyancy forces driving the fluid upwards or downwards [1]. Such double-diffusive processes occur in many fields, including solid-state physics [2] (solidification of binary alloy and crystal growth), oceanography [3] (melting and cooling near a vertical ice surface), geophysics (dispersion of dissolved materials or particulate matter in flows), and others. Because of the coupling between the velocity field and the diffusive scalar fields, double-diffusive convection is more complex than the convection associated with a single diffusive scalar, and many different behaviours may be expected.

The present work is concerned with natural convection along a vertical side wall with imposed horizontal temperature and concentration gradients. Since this problem has attracted much attention [4], it is worth beginning by a short review of the main results which can be found in the literature. Experimentally, only few studies have been devoted to double-diffusive convection with imposed horizontal temperature and concentration gradients along vertical walls [5, 6] or in enclosures [7, 8]. The available experimental results have focused on the measurement of the heat and mass transfers at the wall and they are restricted to a limited range of physical parameters. Theoretically, the governing equations of double diffusion convection are the classical conservation equations for mass, momentum, heat and chemical species [9]. While these are easy to formulate, the existence of two buoyancy forces results in a complicated nonlinear partial derivatives problem. Most of the methods developed in the field of boundary-layer theory [10] have been applied to double-diffusive situations. Among them, the search for similarity solutions attracted much attention, mainly because similarity formulation transforms the transport equations into a set of differential equations which can be solved numerically for different values of the parameters. The existence of similar solutions is now well documented and comprehensive reviews are available in the literature [9, 11, 12]. Other numerical investigations have solved the basic flow equations by finite-difference [13, 14]. In all these approaches, the difficulty resides in getting a physical characterization of the different flow configurations and to achieve valuable predictions for the temperature, concentration and velocity distributions over a wide range of situations. Analytical methods like integral methods [15, 16] and asymptotic expansions [17, 18] have also been used to obtain transport properties as a function of the different parameters involved. The results contain evidence of many different and complicated flows, but the predictions are scarce and restricted to some specific cases. Recently, scale analysis was applied to double diffusive convection in order to determine the heat and mass transfers at the wall [19–22]. The different terms in the equations of motions were estimated from simple order of magnitude arguments and some dominant balances between them were then considered. However, the method, which was based on single-scale analysis, failed to take into account the existence of multiple length scales coupled together and, at the present moment, no satisfactory predictions cover the whole range of parameters.

In this paper, we present a new method that provides a physical understanding of double-diffusive boundary layers and allows us to predict exhaustively the different asymptotic behaviours that can be observed when the relevant parameters are varied. This method combines the use of the integral boundary-layer equations and scaling analysis. Recently, we

## NOMENCLATURE

| | |
|---|---|
| $C$ | chemical species concentration |
| $D$ | chemical species diffusivity |
| $g$ | acceleration of gravity |
| $Le$ | Lewis number $\alpha/D$ |
| $N$ | buoyancy ratio $\beta_C \Delta C/\beta_T \Delta T$ |
| $Nu$ | Nusselt number |
| $Pr$ | Prandtl number $\nu/\alpha$ |
| $Ra_S$ | solutal Rayleigh number $g\beta_C \Delta C x^3/D\nu$ |
| $Ra_T$ | thermal Rayleigh number $g\beta_T \Delta T x^3/\alpha\nu$ |
| $Sc$ | Schmidt number $\nu/D$ |
| $Sh$ | Sherwood number |
| $T$ | temperature |
| $U_C$ | values of the streamwise velocity at $\delta_C$ |
| $U_m$ | value of the streamwise velocity at $\delta_m$ |
| $U_T$ | value of the streamwise velocity at $\delta_T$ |
| $U_\nu$ | value of the streamwise velocity at $\delta_\nu$ |
| $u, v$ | streamwise and spanwise components of the fluid velocity |
| $x, y$ | Cartesian coordinates. |

Greek symbols

| | |
|---|---|
| $\alpha$ | thermal diffusivity of the fluid |
| $\beta_T$ | coefficient of thermal expansion $(-1/\rho)(\partial\rho/\partial T)_p$ |
| $\beta_C$ | coefficient of concentration expansion $(-1/\rho)(\partial\rho/\partial C)_p$ |
| $\gamma$ | dimensionless concentration $(C-C_\infty)/\Delta C$ |
| $\gamma'(0)$ | wall derivative of dimensionless concentration |
| $\delta$ | velocity boundary-layer thickness |
| $\delta_C$ | concentration boundary layer thickness |
| $\delta_m$ | distance to the wall where the velocity is maximum |
| $\delta_T$ | thermal boundary layer thickness |
| $\delta_\nu$ | distance to the wall where viscous friction becomes negligible compared to inertia |
| $\Delta C$ | concentration difference between the wall and infinity $(C_0-C_\infty)$ |
| $\Delta T$ | temperature difference between the wall and infinity $(T_0-T_\infty)$ |
| $\eta$ | similarity variable |
| $\theta$ | dimensionless temperature $(T-T_\infty)/\Delta T$ |
| $\theta'(0)$ | wall derivative of dimensionless temperature |
| $\nu$ | kinematic viscosity |
| $\rho$ | density of fluid |
| $\Phi$ | dimensionless stream function |
| $\Psi$ | stream function. |

Subscripts

| | |
|---|---|
| 0 | condition at the wall |
| $\infty$ | condition at infinity. |

successfully applied this idea to double-diffusive convection in a fluid-filled porous medium [23]. When considering a fluid, as we do here, the higher degree of complexity gives rise to many new and interesting situations.

The paper is organized as follows. In Section 2, we briefly recall the boundary-layer equations for double-diffusive convection near a vertical wall and we present our scaling method; we also introduce similarity equations and we describe the finite-difference method used for solving. In Sections 3 and 4, we focus on the two asymptotic cases which are of physical relevance. Our analysis gives evidence for many different types of flows, each of them being characterized by a particular set of scaling relations. In Section 5, we discuss our results in relation to similarity solutions obtained numerically over a wide range of parameters.

## 2. FORMULATION AND SCALE ANALYSIS

In this paper, we study buoyancy driven flows near an infinitely high half-plate held vertically in an infinite fluid (Fig. 1). The surface of the wall is maintained at a fixed temperature $T_0$ and a fixed concentration $C_0$; the temperature and concentration at infinity are $T_\infty$ and $C_\infty$. The horizontal gradients of $T$ and $C$ inside

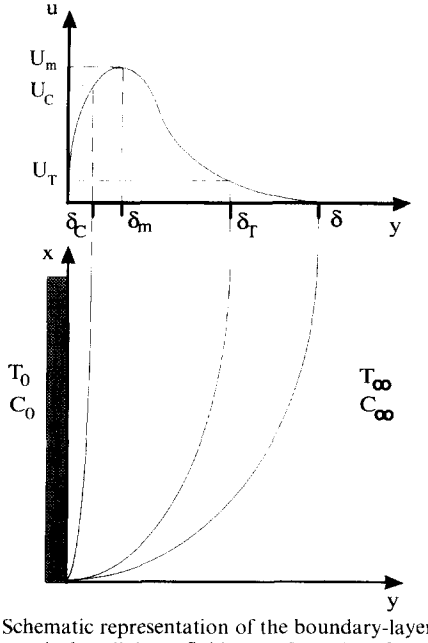


Fig. 1. Schematic representation of the boundary-layer flow near a vertical wall in a fluid ($1 \ll Pr \ll Sc$). $\delta_T$ and $\delta_C$ are the thermal and solutal boundary layer thicknesses. The streamwise velocity is maximum at $\delta_m$ and is zero beyond $\delta$. Physically acceptable configurations must satisfy: $\delta_C \leqslant \delta_T \leqslant \delta$.

the fluid are responsible for density differences which drive the fluid along the wall. The basic governing equations are the conservation of mass, momentum, heat and chemical species. We assume that the density of the fluid is: $\rho = \rho_\infty[1-\beta_T(T-T_\infty)-\beta_C(C-C_\infty)]$. With use of the Boussinesq hypothesis and of the boundary-layer approximation, the equations of motion read [9, 19]

$$\frac{\partial u}{\partial x}+\frac{\partial v}{\partial y}=0 \tag{1a}$$

$$u\frac{\partial u}{\partial x}+v\frac{\partial u}{\partial y}=\nu\frac{\partial^2 u}{\partial y^2}+g\beta_T(T-T_\infty)+g\beta_C(C-C_\infty) \tag{1b}$$

$$u\frac{\partial T}{\partial x}+v\frac{\partial T}{\partial y}=\alpha\frac{\partial^2 T}{\partial y^2} \tag{1c}$$

$$u\frac{\partial C}{\partial x}+v\frac{\partial C}{\partial y}=D\frac{\partial^2 C}{\partial y^2} \tag{1d}$$

$$u(0)=v(0)=u(\infty)=v(\infty)=0;\quad T(0)=T_0;$$
$$C(0)=C_0;\quad T(\infty)=T_\infty;\quad C(\infty)=C_\infty. \tag{1e}$$

The amplitude and the direction of thermal and solutal forces in equation (1b) can be measured by the buoyancy ratio $N$. When $N=0$ and $N=\infty$, we recover the case where a single scalar is diffusing; when $N<0$, thermal and solutal forces drive the flow in opposite directions and the flow field can reverse; when $N>0$, buoyancy forces are cooperating and drive the flow in the same direction. In the present study, the flows are laminar and $N \geqslant 0$.

The description of the distributions of temperature, concentration and velocity in the fluid involves several horizontal length scales which are sketched in Fig. 1. $T$ and $C$ decrease from their values on the wall to their values at infinity over the characteristic length scales $\delta_T(x)$ and $\delta_C(x)$; the velocity takes the values $U_T$ and $U_C$, respectively in $\delta_T$ and $\delta_C$. The streamwise velocity $u$ increases from 0 on the wall to its maximum value $U_m$ at $\delta_m(x)$, then decreases and vanishes at $\delta(x)$. We also introduce $\delta_v(x)$ which characterizes the distance where viscous friction becomes negligible in comparison with inertia.

The aim of this paper is to predict all the solutions of the set of equations (1) when $N$ and the diffusion coefficients are varied. It will be convenient to use the parameters $Pr$, $Sc$ and $Le$. Their values depend on the nature of the fluid and on the physical mechanisms governing the diffusion of the heat and chemical species. In gases, we have $\nu \cong \alpha \cong D$, leading to $Pr$, $Sc$ and $Le$ being of the order of 1. In most liquids, the Prandtl and Schmidt numbers are greater than unity, except in molten metals, where the Prandtl number is less than unity. Usually, heat diffusion is more efficient than mass diffusion, yielding a Lewis number greater than 1. Typical values of $Le$ in common solutions are about 100; but $Le$ can be very large in complex solutions containing macromolecules or colloidal dispersions. Since $Pr$, $Sc$ and $Le$ are related through $Le = Sc/Pr$, we see that only two physical cases fit the requirement $Le > 1 : Pr < 1 < Sc$ (molten metals) and $1 < Pr < Sc$ (solutions).

Table 1. Summary of the different scales involved in the analysis of pure thermal convection at low and high Prandtl numbers (ref. [19], Chap. 4). Since the length scales are all proportional to $x[Ra_T(x)]^{-1/4}$ and the velocity scales to $\alpha[Ra_T(x)]^{1/2}/x$, we have omitted these factors and the table gives only the multiplicative coefficients

| | $\delta_m$ | $U_m$ | $\delta$ |
|---|---|---|---|
| $Pr \ll 1$[a] | $Pr^{1/4}$ | $Pr^{1/2}$ | $Pr^{-1/4}$ |
| $Pr \gg 1$[b] | 1 | 1 | $Pr^{1/2}$ |

[a] $\delta_v = \delta_m$; $\delta_T = \delta$. [b] $\delta_v = \delta$; $\delta_T = \delta_m$.

We first note that when $Pr = Sc$, equations (1a–e) reduce to those for a single buoyancy effect.This problem has been extensively analysed and it will not be treated here since the results are now classical (see for instance ref. [19], chap. 4). In Table 1, we just recall the properties of thermal convection at low and high Prandtl numbers which will be useful in the following discussion. Only two horizontal length scales are involved, $\delta_m$ and $\delta$, which define an inner and an outer sublayer; the velocity scale $U_m$ suffices to characterize the velocity field. When $Pr \neq Sc$, the length scales $\delta_T$, $\delta_C$, $\delta_m$, $\delta$ and $\delta_v$ are in general different and there exist different velocity scales, $U_C$, $U_T$, $U_m$, $U_v$; as a consequence of these multiple scales, the flow along the wall splits into several sublayers, each with a characteristic thickness and a characteristic velocity scale. This precludes any straightforward estimate of the different terms appearing in the conservation equation from simple order of magnitude arguments, as it is done in pure thermal convection.

Our scaling method proceeds as follows. First, we specify the different sublayers which are to be considered and the relevant length and velocity scales. Then, we rewrite the conservation equations under their integral form, combining the incompressibility relation (1a) with the three other equations and integrating across a volume control $[y_1, y_2]$. It is convenient to express these equations in terms of the dimensionless temperature and concentration, $\theta$ and $\gamma$:

$$\int_{y_1}^{y_2}\frac{\partial(u^2)}{\partial x}\,dy+u(y_2)v(y_2)-u(y_1)v(y_1)$$
$$=\nu\left\{\left.\frac{\partial u}{\partial y}\right|_{y_2}-\left.\frac{\partial u}{\partial y}\right|_{y_1}\right\}+g\beta_T\Delta T\int_{y_1}^{y_2}(\theta+N\gamma)\,dy \tag{2a}$$

$$\int_{y_1}^{y_2} \frac{\partial (u\theta)}{\partial x} \mathrm{d}y + v(y_2)\theta(y_2) - v(y_1)\theta(y_1) = \alpha \left\{ \left. \frac{\partial \theta}{\partial y} \right|_{y_2} - \left. \frac{\partial \theta}{\partial y} \right|_{y_1} \right\} \quad (2b)$$

$$\int_{y_1}^{y_2} \frac{\partial (u\gamma)}{\partial x} \mathrm{d}y + v(y_2)\gamma(y_2) - v(y_1)\gamma(y_1) = D \left\{ \left. \frac{\partial \gamma}{\partial y} \right|_{y_2} - \left. \frac{\partial \gamma}{\partial y} \right|_{y_1} \right\}. \quad (2c)$$

In practice, we choose $[y_1, y_2]$ so that $y_1$ and $y_2$ coincide with the boundaries of the sublayers, i.e. 0, $\delta_C$, $\delta_T$, $\delta_m$, $\delta_v$ or $\delta$. Then, we estimate the orders of magnitude of the terms appearing in system (2) taking for $u$, $v$, $\theta$ and $\gamma$, the characteristic values which are appropriate in $[y_1, y_2]$. The same procedure is applied to the sublayers at hand and we get a system of nonlinear algebraic equations whose unknowns are the relevant scales of the problem. Considering the different possible leading-order balances in these equations and solving, we find out all the possible flow configurations when $N$, $Pr$ and $Sc$ are varied. In this method, the advantage of starting from integral equations is that each sublayer is analysed separately; the contributions of the different terms appearing in the conservation equations are taken at the boundaries of the sublayer which preserves the coupling between the different sublayers. This method is applied to the study of double-diffusive convection for $1 \ll Pr \ll Sc$ and $Pr \ll 1 \ll Sc$ in Sections 3 and 4.

To test the validity of our results, we shall compare our predictions with similarity solutions of the boundary-layer equations, in Section 5. Setting $\eta = y[Ra_T(x)]^{1/4}/x$ and $\Psi(\eta) = \alpha[Ra_T(x)]^{1/4}\Phi(\eta)$, we get [9]

$$\Phi''' + 3\Phi\Phi'' - 2\Phi'^2 + (\theta + N\gamma) = 0 \quad (3a)$$

$$\theta'' + 3Pr\Phi\theta' = 0 \quad (3b)$$

$$\gamma'' + 3Sc\Phi\gamma' = 0 \quad (3c)$$

$$\theta(0) = \gamma(0) = 1; \quad \Phi(0) = 0; \quad \theta(\infty) = \gamma(\infty) = 0. \quad (3d)$$

We solve this system by finite-differences with an adaptive stepsize procedure to account for the fact that $\theta$ and $\gamma$ decrease over very different length scales [24]. Near the wall, the stepsize $\Delta\eta$ is very small (typically $\Delta\eta \cong 10^{-3}$ when $Le = 10^5$), to achieve a good determination of the thin concentration boundary-layer, and it increases steadily with $\eta$. Integration is performed over a finite segment $[0, \eta_{max}]$. The boundary conditions are satisfied when the differences between the exact boundary conditions (3d) and the values calculated at $\eta_{max}$ are smaller than $10^{-6}$. Then, the length of the segment of integration, $\eta_{max}$, is increased until the difference at any point between two successive solutions is smaller than $10^{-6}$ (typically $\eta_{max} \cong 200$ when $Pr = 10^2$).

## 3. SCALE ANALYSIS OF DOUBLE-DIFFUSIVE CONVECTION FOR $1 \ll Pr \ll Sc$

In this section, we apply the scaling method presented in the previous section to study double-diffusive convection in the asymptotic case $1 \ll Pr \ll Sc$. We first note that some useful relations can be found between $\delta_m$, $\delta$, $\delta_v$, $\delta_C$ and $\delta_T$ prior to any calculation. We have $\delta_C \ll \delta_T$ as a consequence of $Le \gg 1$. Secondly, on the basis of the scaling of pure thermal convection (Table 1), we argue that $Pr \gg 1$ imply that $\delta_1 \ll \delta$ and $\delta_v = \delta$. If solutal convection were the only driving mechanics, the streamwise velocity would reach maximum at $\delta_m = \delta_C$, since $Sc \gg 1$ (ref. [19], p. 117). In the opposite case where thermal buoyancy works alone, we should have $\delta_m = \delta_T$. Therefore, the location of $\delta_m$ results from a competition between solutal and thermal effects. Finally, we can divide the flow into several sublayers, each with a different combination of leading mechanisms:

(1) in $[0, \delta_C]$, on the basis of single diffusive convection, the flow must be ruled by friction, solutal and thermal buoyancy, since $Sc \gg 1$;

(2) in $[\delta_C, \delta_T]$, we cannot decide beforehand whether friction is balanced by advection or by thermal buoyancy; in the following, we shall examine both possibilities;

(3) in $[\delta_T, \delta]$, the terms to be retained are advection and friction, since $Pr \gg 1$.

Let us first consider that a balance between friction and thermal buoyancy holds in layer $[\delta_C, \delta_T]$. Since advection is negligible below $\delta_T$, we anticipate that $u$ reaches its maximum at $\delta_m = \delta_T$. In addition, we assume that $U_T \gg U_C$ or perhaps $U_T \approx U_C$. The velocity scales are $U_C$ in layer $[0, \delta_C]$, and $U_T$ in $[\delta_C, \delta_T]$. Expressing the conservation of momentum, heat and chemical species, we get (see the Appendix)

$$U_C \approx \frac{g\beta_T \Delta T}{\nu}(\delta_T + N\delta_C)\,\delta_C \quad (4a)$$

$$U_T \approx \frac{g\beta_T \Delta T}{\nu}(\delta_T^2 + N\delta_C^2) \quad (4b)$$

$$U_T \approx \frac{\alpha x}{\delta_T^2} \quad (4c)$$

$$U_C \approx \frac{Dx}{\delta_C^2} \quad (4d)$$

$$U_T \approx \frac{\nu x}{\delta^2}. \quad (4e)$$

Let us solve system (4) analytically. This will lead us to introduce different asymptotic cases, each corresponding to distinct flow properties. For clarity, we shall summarize the scaling laws in Table 2 and we

Table 2. Summary of the different scales involved in double-diffusive convection when $1 \ll Pr \ll Sc$. From Section 3, the length scales are all proportional to $x[Ra_T(x)]^{-1/4}$ and the velocity scales to $\alpha[Ra_T(x)]^{1/2}/x$. For clarity we have omitted these factors and the table gives only the multiplicative coefficients

| | $\delta_C$ | $U_C$ | $\delta_T$ | $U_T$ | $\delta_v = \delta$ |
|---|---|---|---|---|---|
| Type 1[a] $N \ll Pr^{-1/3}Sc^{1/3}$ | $Pr^{1/3}Sc^{-1/3}$ | $Pr^{1/3}Sc^{-1/3}$ | 1 | 1 | $Pr^{1/2}$ |
| Type 2[a] $Pr^{-1/3}Sc^{1/3} \ll N \ll Pr^{-1}Sc$ | $N^{-1/4}Pr^{1/4}Sc^{-1/4}$ | $N^{1/2}Pr^{1/2}Sc^{-1/2}$ | — | — | — |
| Type 3[b] $Pr^{-1}Sc \ll N \ll Sc$ | — | — | $N^{-1/4}Pr^{-1/4}Sc^{1/4}$ | $N^{1/2}Pr^{1/2}Sc^{-1/2}$ | $N^{-1/4}Pr^{1/4}Sc^{1/4}$ |
| Type 4[c] $N \gg Sc$ | — | — | — | — | — |

[a] $\delta_m = \delta_T$; $U_m = U_T$. [b] $\delta_m = \delta_T$; $U_m = U_T = U_C$. [c] $\delta_m = \delta_C$; $U_m = U_C$.

shall locate the different types of flows in the three-dimensional diagram $(N, Pr, Sc)$ reproduced in Fig. 2. Equation (4a) splits into two parts depending on the value of $N$.

$N \ll \delta_T/\delta_C$. We neglect $N\delta_C$ on the right hand side of equation (4a), $N\delta_C^2$ in equation (4b) since $N\delta_C^2 \ll \delta_T\delta_C \ll \delta_T^2$, and we easily derive a set of values for $\delta_C$, $\delta_T$, $\delta$, $U_C$ and $U_T$, which is reported in Table 2. To establish the relevance of these scales, we check that $\delta_C$, $\delta_T$ and $\delta$ satisfy the inequality $\delta_C \ll \delta_T \ll \delta$, that the flow in layer $[\delta_C, \delta_T]$ is well controlled by the interplay between thermal buoyancy and friction, and that we have $U_C \ll U_T$. Finally $N \ll \delta_T/\delta_C$ requires that $N \ll Le^{1/3}$. In the following, it will be convenient to use parameters $Pr$ and $Sc$ and to write $N \ll Pr^{-1/3}Sc^{1/3}$. These flows will be called flows of type 1 from now on. In the three-dimensional diagram $(N, Pr, Sc)$ depicted in Fig. 2, flows of type 1 are located behind the surface $N = Pr^{-1/3}Sc^{1/3}$; the different scaling relations are reported in Table 2.

$N \gg \delta_T/\delta_C$, i.e. $N \gg Pr^{-1/3}Sc^{1/3}$. $U_C$ results from solutal buoyancy in layer $[0, \delta_T]$. In equation (4a), we set $\delta_T \ll N\delta_C$; the form of equation (4b) leads us to consider separately two subcases depending on the relative values of $N\delta_C^2$ and $\delta_T^2$. When $N\delta_C^2 \ll \delta_T^2$, we get a set of solutions which characterise flows of type 2 (Table 2). We check easily that $U_T$ is much larger than $U_C$ and that viscous friction dominates over inertia as required; condition $N\delta_C^2 \ll \delta_T^2$ requires that $N \ll Pr^{-1}Sc$. In Fig. 2, flows of type 2 are located in the domain between $N = Pr^{-1/3}Sc^{1/3}$ and $N = Pr^{-1}Sc$. When $N\delta_C^2 \gg \delta_T^2$, i.e. $N \gg Pr^{-1}Sc$, $U_T$ is of the same order of magnitude as $U_C$, but the reasoning upon which system (4) was derived remains valid, provided that inertia is negligible compared with friction in layer $[\delta_C, \delta_T]$, which requires $N \ll Sc$. These solutions, which are valid for $Pr^{-1}Sc \ll N \ll Sc$, characterize flows of type 3 (Table 2 and Fig. 2).

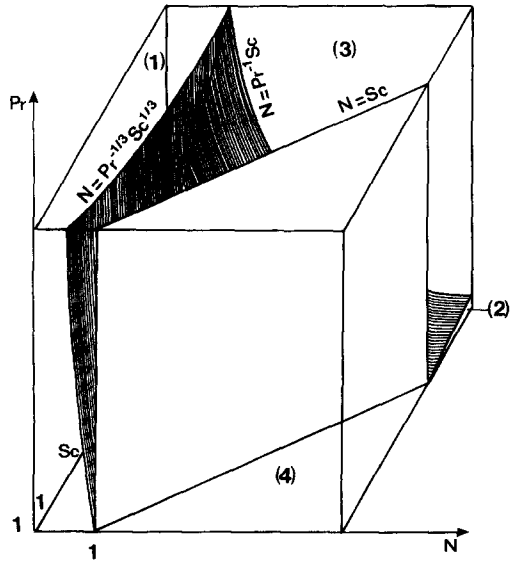


Fig. 2. Different asymptotic types of flow occurring as a function of parameters $N$, $Pr$ and $Sc$ when $1 \ll Pr \ll Sc$.

When $N \gg Sc$, the interplay between friction and thermal buoyancy is no longer appropriate in layer $[\delta_C, \delta_T]$, and system (4) fails. Therefore, we now consider that the flow in $[\delta_C, \delta_T]$ results from a competition between friction and inertia. Since advection restrains the flow above $\delta_C$, $\delta_m$ must be equal to $\delta_C$. The flow in $[0, \delta_C]$ is ruled by a balance between friction and solutal buoyancy; in $[\delta_C, \delta]$, it results from friction and inertia. Thermal effects are negligible and solutal convection works alone. The velocity field involves only two length scales, $\delta_C$ and $\delta$, and one velocity scale, $U_C$. These flows will be said to be of type 4. The analysis can be carried out just as in single diffusive convection. $U_C$, $\delta_C$ and $\delta$ are obtained from Table 1, replacing $Pr$, $\alpha$ and $Ra_T$ by $Sc$, $D$ and $Ra_S = Ra_T LeN$. The conservation of heat in $[0, \delta_T]$, where the velocity scale is $U_C$, yields $U_C\delta_T/x \approx \alpha/\delta_T$, which gives a solution for $\delta_T$. Since $U_C$ is the sole velocity scale, we must have: $U_C/(\delta - \delta_C) \approx U_T(\delta - \delta_T)$, or $U_T \approx U_C$. In Table 2, we see that flows of type 4 are characterized by the same scaling relations as type 3 flows, even though they result from different combinations of leading mechanisms.

Summarizing, we have derived the four types of flows which are expected in the asymptotic case $1 \ll Pr \ll Sc$. These flow configurations are the only asymptotic solutions that can be found and it is easily verified that all the assumptions upon which they have been established are satisfied. Inversely, any other

combination of scales and leading mechanisms turns out to be inconsistent. It is worth noting that the length scales are all proportional to $x[Ra_T(x)]^{-1/4}$ and the velocity scales to $\alpha[Ra_T(x)]^{1/2}/x$ which justifies the form of the similarity variable $\eta$ and that of the stream function $\Psi$ in the previous section. In Section 5, these results will be discussed in relation to the similarity solutions obtained numerically.

## 4. SCALE ANALYSIS OF DOUBLE DIFFUSIVE CONVECTION FOR $Pr \ll 1 \ll Sc$

This case is more complex than the previous one, yielding new modes of interaction between thermal and solutal effects. Our scaling is based still on the existence of the multiple length scales, $\delta_m$, $\delta$, $\delta_v$, $\delta_T$, $\delta_C$, which here verify $0 \ll \delta_C \ll \delta_v \ll \delta = \delta_T$. Indeed, $Le \gg 1$ implies that $\delta_C \ll \delta_T$, while on the basis of thermal convection (Table 1), we infer from $Pr \ll 1$ and $Sc \gg 1$ that $\delta_v \ll \delta = \delta_T$ and $\delta_C \ll \delta_v$. Therefore, we have: $\delta_C \ll \delta_v \ll \delta = \delta_T$ and the flow along the wall splits into three distinct layers as a function of the wall distance:

(1) $[0, \delta_C]$ where the leading mechanisms are viscous friction, thermal and solutal buoyancy since $Sc \gg 1$;

(2) $[\delta_C, \delta_v]$ where the leading mechanisms may be either friction and thermal buoyancy or friction and inertia—these two physical situations will be examined separately;

(3) $[\delta_v, \delta]$ where the flow results from a balance between inertia and thermal buoyancy since $Pr \ll 1$.

Let us first consider that the leading mechanisms in $[\delta_C, \delta_v]$ are friction and thermal buoyancy. Advection, which is responsible for the decrease of momentum, only acts in layer $[\delta_v, \delta]$. Therefore, we anticipate that the streamwise velocity necessarily reaches its maximum at $y \approx \delta_v$ and then decreases: $\delta_m = \delta_v$ and $U_m = U_v$. We also assume that $U_v \gg U_C$ or possibly $U_v \approx U_C$. $U_C$ and $U_v$ are the velocity scales, respectively, in $[0, \delta_C]$ and in $[\delta_C, \delta_T]$. Once expressed in terms of the suitable scales, equations (2a–c) yield (the calculations are detailed in the Appendix):

$$U_C \approx \frac{g\beta_T \Delta T}{\nu}(\delta_v + N\delta_C)\,\delta_C \tag{5a}$$

$$U_v - U_C \approx \frac{g\beta_T \Delta T}{\nu}\delta_v^2 \tag{5b}$$

$$U_v^2 \approx g\beta_T \Delta T x \tag{5c}$$

$$U_v \approx \frac{\alpha x}{\delta_T^2} \tag{5d}$$

$$U_C \approx \frac{Dx}{\delta_C^2}. \tag{5e}$$

When the flow in $[\delta_C, \delta_v]$ is governed by a balance between friction and inertia, we expect that the streamwise velocity will reach its maximum at $y \approx \delta_C$, so that $\delta_m = \delta_C$ and $U_m = U_C \gg U_v$. $U_C$ and $U_v$ are the velocity scales in $[0, \delta_C]$ and in $[\delta_C, \delta_T]$. The conservation equations under their integrals forms give (see the Appendix)

$$U_C \approx \frac{g\beta_T \Delta T}{\nu}(1+N)\,\delta_C^2 \tag{5'a}$$

$$U_v^2 \approx g\beta_T \Delta T x \tag{5'b}$$

$$U_C\delta_v + U_v\delta_T \approx \frac{\alpha x}{\delta_T} \tag{5'c}$$

$$U_C \approx \frac{Dx}{\delta_C^2} \tag{5'd}$$

$$U_C \approx \frac{\nu x}{\delta_v^2}. \tag{5'e}$$

We now solve these two sets of equations beginning with system (5). From equation (5a), we distinguish two situations depending on the value of $N$ compared with the ratio $\delta_v/\delta_C$.

$N \ll \delta_v/\delta_C$. Solving system (5) with $U_C \approx g\beta_T \Delta T \delta_v \delta_C/\nu$, we derive a first set of solutions for $\delta_C$, $U_C$, $\delta_v$, $U_v$ and $\delta$ which is reported in Table 3. These scaling properties characterize a type of flow, which for convenience will be said to be of type 1. We check that $U_v = U_m \gg U_C$ and $\delta_C \ll \delta_v \ll \delta$. Inertia is of the same order as friction, but this does not change the scaling. $N \ll \delta_v/\delta_C$ translates into $N \ll Sc^{1/3}$; in Fig. 3, flows of type 1 occupy the domain located behind the surface $N = Sc^{1/3}$.

$N \gg \delta_v/\delta_C$ i.e. $N \gg Sc^{1/3}$. $U_C$ is now imposed by solutal buoyancy: $U_C \approx g\beta_T \Delta T N \delta_C^2/\nu$ and system (5) admits new solutions. We check that friction and thermal buoyancy are the leading mechanisms within

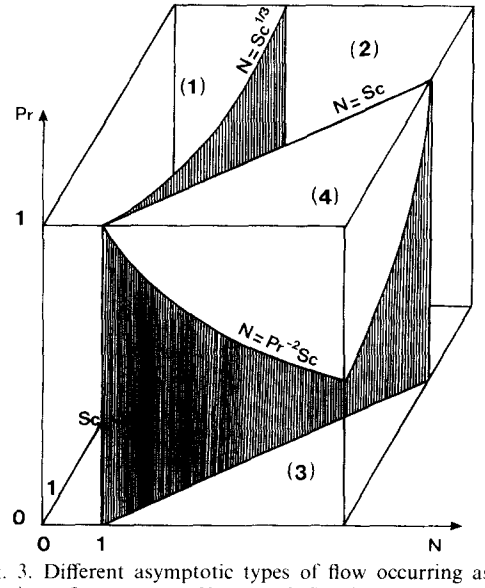


Fig. 3. Different asymptotic types of flow occurring as a function of parameters $N$, $Pr$ and $Sc$ when $Pr \ll 1 \ll Sc$. Note the continuity between this diagram and that in Fig. 2.

Table 3. Summary of the different scales involved in double-diffusive convection when $Pr \ll 1 \ll Sc$. From Section 4, the length scales are all proportional to $x[Ra_T(x)]^{-1/4}$ and the velocity scales to $\alpha[Ra_T(x)]^{1/2}/x$; the table only gives the multiplicative coefficients

| | $\delta_C$ | $U_C$ | $\delta_v$ | $U_v$ | $\delta_T = \delta$ |
|---|---|---|---|---|---|
| Type 1[a] $N \ll Sc^{1/3}$ | $Pr^{1/4}Sc^{-1/3}$ | $Pr^{1/2}Sc^{-1/3}$ | $Pr^{1/4}$ | $Pr^{1/2}$ | $Pr^{-1/4}$ |
| Type 2[a] $Sc^{1/3} \ll N \ll Sc$ | $N^{-1/4}Pr^{1/4}Sc^{-1/4}$ | $N^{1/2}Pr^{1/2}Sc^{-1/2}$ | — | — | — |
| Type 3[b] $Sc \ll N \ll Pr^{-2}Sc$ | — | — | $N^{-1/4}Pr^{1/4}Sc^{1/4}$ | — | — |
| Type 4[b] $N \gg Pr^{-2}Sc$ | — | — | — | — | $N^{-1/4}Pr^{-3/4}Sc^{1/4}$ |

[a] $\delta_m = \delta_v$; $U_m = U_v$. [b] $\delta_m = \delta_C$; $U_m = U_C$.

$[\delta_C, \delta_v]$, as required if $N$ and $Sc$ verify the additional requirement $N \ll Sc$. Thus, we must consider separately the two following possibilities. When $Sc^{1/3} \ll N \ll Sc$, we get flows of type 2 (Table 3). In Fig. 3, these flows are located in the domain between $N = Sc^{1/3}$ and $N = Sc$. When $N \gg Sc$, the flow in layer $[\delta_C, \delta_v]$ cannot be dictated by a balance between friction and thermal buoyancy and system (5) is no longer valid.

When $N \gg Sc$, we consider that the leading mechanisms are friction and inertia so that we have to solve system (5′). Since $N \gg Sc \gg 1$, the right-hand side of (5′a) reduces to: $U_C \approx g\beta_T \Delta T N \delta_C^2/\nu$. Equations (5′a), (5′b), (5′d) and (5′e) give directly $U_C$, $\delta_C$, $U_v$ and $\delta_v$. Equation (5′c) yields two different asymptotic behaviours for $\delta_T$, depending on which contribution to heat transfer predominates:

(a′) $U_C\delta_v \ll U_v\delta_T$: the main contribution to heat transfer here comes from advection in $[\delta_v, \delta_T]$. These flows are said to be of type 3 (Table 3).

(b′) $U_C\delta_v \gg U_v\delta_T$: heat advection in $[\delta_C, \delta_v]$ prevails, yielding flows of type 4 (Table 3).

We can easily verify that these two asymptotic solutions satisfy the different conditions upon which system (5′) was established. The cross-over between types 3 and 4 occurs for $N = Pr^{-2}Sc$. In Fig. 3, flows of type 3 and 4 are located in front of the plane $N = Sc$ on both sides of the surface $N = Pr^{-2}Sc$.

## 5. DISCUSSION

### 5.1. *Velocity, temperature and concentration distributions*

We are now in a position to discuss the results of the asymptotic analyses reported in Section 3 and 4 in relation to similarity solutions obtained numerically over a wide range of parameters. Several common properties emerge from the scaling relations listed in Tables 2 and 3 and from the distributions of velocity, temperature and concentration which are reported in Figs. 4 and 5.

Let us begin with flows of type 1. From Tables 2 and 3, we expect flows of type 1 to be heat driven. Indeed, the velocity and temperature fields vary as in pure thermal convection. The concentration fields are entirely determined by thermal effects and the solutal forces have no action on the flows. The problem involves only two length scales, namely $\delta_T$ and $\delta$ when $Pr \gg 1$ or $\delta_v$ and $\delta_T$ when $Pr \ll 1$. In Figs. 4a and 5a, we checked that the streamwise velocity and the temperature coincide exactly with the velocity and the temperature in pure thermal convection at the same Prandtl numbers. In the three-dimensional diagrams depicted in Figs. 2 and 3, this result is expressed by the fact that flows of type 1 are located in contiguous domains connected to each other through the plane $Pr = 1$. We emphasize that heat driven flows can be observed for $N \gg 1$, i.e. they include flows where the amplitude of solutal forces dominates over that of thermal forces.

Flows of type 2, 3 and 4 are driven by a combination of thermal and solutal effects, except flows of type 4 when $Pr \gg 1$ which are entirely mass driven. The velocity distributions involve three length scales: $\delta_C$, $\delta_T$ and $\delta$ when $Pr \gg 1$, $\delta_C$, $\delta_v$ and $\delta_T$ when $Pr \ll 1$. It is worth expressing $\delta_C$ and $U_C$ in terms of $D$, $Ra_S$ and $Sc$ instead of $\alpha$, $Ra_T$, $N$, $Pr$ and $Sc$. We see immediately that $\delta_C \approx x[Ra_S(x)]^{-1/4}$ and $U_C \approx Dx^{-1}[Ra_S(x)]^{-1/4}$ scale as in pure solutal convection, reflecting the fact that the transport of chemical species is now ruled by solutal convection only and that it is not coupled with thermal convection.

Let us first examine the type 2 flows. In Tables 2 and 3, the different scales, $\delta_T$, $\delta$ and $U_T$ on the one hand, and $\delta_v$, $\delta_T$ and $U_v$ on the other hand, are clearly the same as in pure thermal convection. Therefore, we expect the fluid motion to be mass driven in $[0, \delta_C]$ and heat driven in $[\delta_C, \delta_T]$. This is perfectly corroborated by the computations. Indeed, in Figs. 4b and 5b, the streamwise velocities have the same variations as in pure thermal convection, except near the wall where they are determined by solutal convection; the temperature distributions coincide with those in pure thermal convection. As previously described, the fact that the type 2 flows for $Pr \gg 1$ and $Pr \ll 1$ have common properties is reflected by their location in contiguous domains of the $(N, Pr\,Sc)$ diagrams represented in Figs. 2 and 3.

In types 3 and 4, the solutal forces are so large

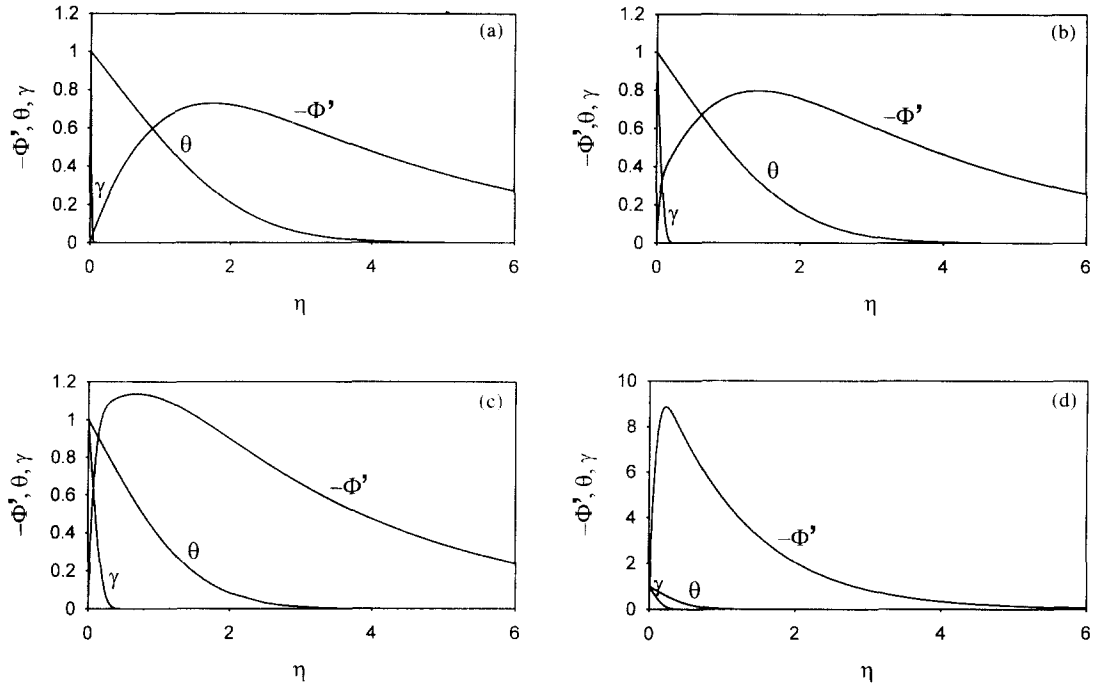


Fig. 4. $-\Phi'$, $\theta$, $\gamma$ as functions of $\eta$ for different values of $N$, $Pr$ and $Sc$ ($Pr > 1$). (a) $N = 5$, $Pr = 10$, $Sc = 1.25 \times 10^6$; (b) $N = 10^2$, $Pr = 10$, $Sc = 10^4$; (c) $N = 10^2$, $Pr = 10$, $Sc = 10^3$; (d) $N = 10^4$, $Pr = 10$, $Sc = 10^2$.

compared with the amplitude of the thermal forces that the streamwise velocity reaches its maximum at $\delta_C$. The interaction between the thermal and solutal effects is more complex than in flows of types 1 and 2, yielding several new features. Let us first consider flows of type 3. In Figs. 2 and 3, the domains of existence for type 3 flows are totally disconnected, yielding distinct properties. When $Pr \gg 1$, a close examination of Table 2 shows that $U_T \approx U_C$ and $\delta_1 \approx \delta_C (Sc/Pr)^{1/2}$: moreover, $\delta \approx x[Ra_S(x)]^{-1/4} Sc^{1/2}$

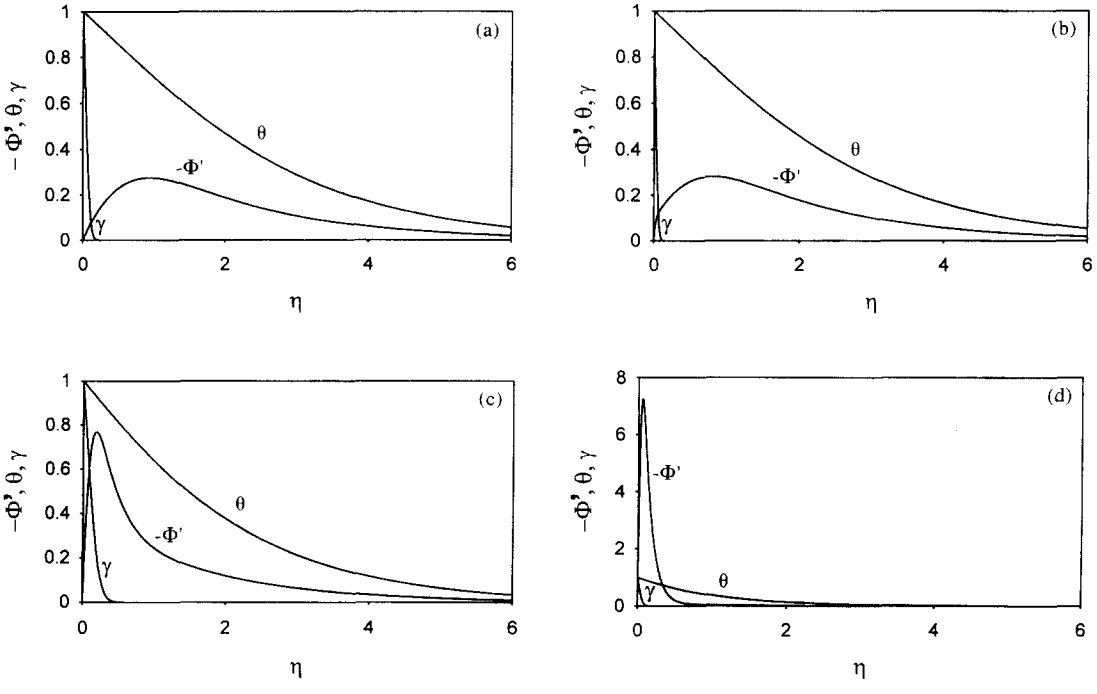


Fig. 5. $-\Phi'$, $\theta$, $\gamma$ as functions of $\eta$ for different values of $N$, $Pr$ and $Sc$ ($Pr < 1$). (a) $N = 5$, $Pr = 0.1$, $Sc = 10^3$; (b) $N = 10^2$, $Pr = 0.1$, $Sc = 10^3$; (c) $N = 10^2$, $Pr = 0.1$, $Sc = 10$; (d) $N = 10^4$, $Pr = 0.1$, $Sc = 10$.

scales as if solutal convection were acting alone (Table 1). We conclude that the fluid motion is mass driven in $[0, \delta_C]$ and $[\delta_T, \delta]$, but that in $[\delta_C, \delta_T]$ it is driven by a combination of thermal and solutal effects. This agrees with the results of Fig. 4c where the velocity is mass driven near the wall, peaks on a flat plateau reflecting the fact that $U_T$ has the same order of magnitude as $U_C$ in the scale analysis, and then decreases to zero. The temperature boundary-layer thickness is shorter than in pure thermal convection because of the coupling between heat and mass convection. When $Pr \ll 1$, the flow properties are different. $\delta_v \approx x[Ra_S(x)]^{-1/4}Sc^{1/2}$ scales as the velocity boundary-layer thickness $\delta$ in pure solutal convection (Table 1). This shows that the fluid motion switches from mass-driven convection to heat-driven convection at $\delta_v$. The main contribution to heat transfer comes from advection in $[\delta_v, \delta_T]$, which is itself heat driven so that $\delta_T$ scales as in pure thermal convection. These predictions are in perfect agreement with Fig. 5c where the temperature distribution and the velocity above $\delta_v$ are very close to the solutions expected for pure thermal convection.

Lastly, flows of type 4, which in Figs. 2 and 3 are located in contiguous regions separated by the plane $Pr = 1$, also resemble one another (Figs. 4d and 5d), except that the coupling between the thermal and solutal effects for $Pr \ll 1$ and $Pr \gg 1$ are somewhat different. When $Pr \gg 1$, solutal convection works alone. Fluid motion is entirely mass driven; the temperature field is determined by solutal effects only and it has no reverse action on the flow. When $Pr \ll 1$, the velocity field is mass driven in $[0, \delta_v]$ and heat driven above $\delta_v$. Heat transport, which arises mainly from advection in $[\delta_C, \delta_v]$, is coupled with solutal convection, and the thermal boundary-layer thickness is much shorter than if thermal convection were working alone.

### 5.2. *Heat and mass transfer*

As a consequence of the complex interaction between thermal and solutal forces, the cross-overs between these different flow types are not trivial and cannot be found *a priori* from simple order-of-magnitude arguments. For instance, the transfer of chemical species switches from heat-driven mass transfer to mass-driven mass transfer for $N = Pr^{-1/3}Sc^{1/3}$, when $Pr \gg 1$ and $N = Sc^{1/3}$, when $Pr \ll 1$, and not simply for $N = 1$. This result was first recognized in refs. [19–21] on the basis of a simplified scale analysis. In the same manner, Tables 2 and 3 show that the transition between heat transfer ruled by thermal convection and heat transfer ruled by solutal convection occurs for $N = Pr^{-1}Sc$, when $Pr \gg 1$, and $N = Pr^{-2}Sc$, when $Pr \ll 1$. The validity of our predictions is tested in Figs. 6 and 7, where we have represented the wall derivatives of $\theta$ and $\gamma$. $|\theta'(0)|$ and $|\gamma'(0)|$, which scale as $1/\delta_T$ and $1/\delta_C$, provide a quantitative way of testing the predictions of the scale analysis. Numerically, $\theta'(0)$ and $\gamma'(0)$ are taken at the first interval of integration. The relative error $|\theta'(0)|$ and $|\gamma'(0)|$ is lower than $10^{-3}$.

Figure 6a is a log–log representation of $|\theta'(0)|$ as a function of $NPrSc^{-1}$; it shows a perfect agreement with the predictions reported in Table 2. Provided that the ratio $Sc/Pr$ is large enough (empty symbols), the numerical data fall on a universal curve with a very good approximation. When $NPrSc^{-1} \ll 1$, the flows are heat-driven, heat transfer is governed entirely by thermal convection and $|\theta'(0)|$ does not

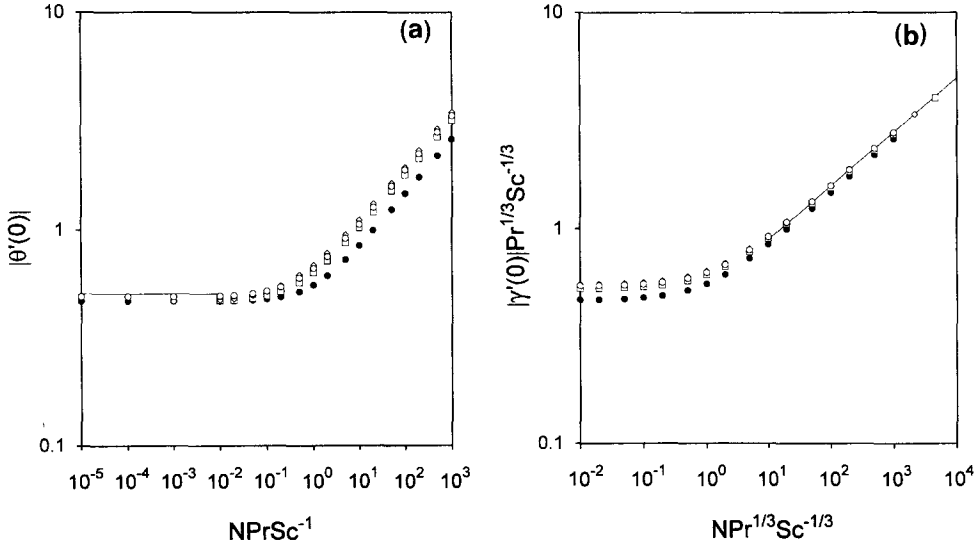


Fig. 6. Log–log representation of $|\theta'(0)|$ as a function of the ratio $NPrSc^{-1}$ (left), of $|\gamma'(0)|\ Pr^{1/3}Sc^{-1/3}$ as a function of $NPr^{1/3}Sc^{-1/3}$ (right). The symbols refer to different values of the physical parameters: $Pr = 10$ and $Sc = 10$ (●); $Pr = 10$ and $Sc = 10^2$ (□); $Pr = 10$ and $Sc = 10^3$ (◇); $Pr = 10^2$ and $Sc = 10^3$ (○). The lines represent the variations of $|\theta'(0)|$ and $|\gamma'(0)|Pr^{1/3}Sc^{-1/3}$, respectively, in the asymptotic limits $N = 0$, $Pr = \infty$ and $N = \infty$, $Sc = \infty$.

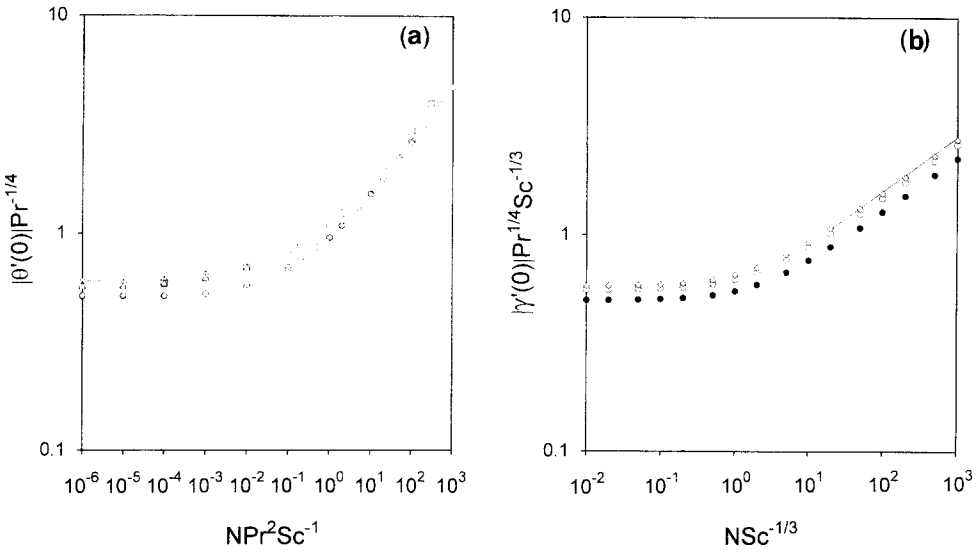


Fig. 7. Log–log representation of $|\theta'(0)|Pr^{-1/4}$ as a function of $NPr^2Sc^{-1}$ (left), of $|\gamma'(0)|\ Pr^{1/4}Sc^{-1/3}$ as a function of $NSc^{-1/3}$ (right). The symbols refer to different values of the physical parameters: $Pr = 10^{-1}$ and $Sc = 1$ (●); $Pr = 10^{-1}$ and $Sc = 10$ (○); $Pr = 10^{-1}$ and $Sc = 10^2$ (◇); $Pr = 10^{-2}$ and $Sc = 10$ (□); $Pr = 10^{-2}$ and $Sc = 10^2$ (△); $Pr = 10^{-3}$ and $Sc = 10$ (×). The lines represent the variations of $|\theta'(0)|Pr^{-1/4}$ and $|\gamma'(0)|Pr^{1/4}Sc^{-1/3}$, respectively, in the asymptotic limits $N = 0$, $Pr = 0$ and $N = \infty$, $Sc = \infty$.

depend on $N$, $Pr$ and $Sc$. As $Pr$ increases, the points calculated numerically tend towards the same limit as in pure thermal convection for $N = 0$ and $Pr = \infty$ ($|\theta'(0)| = 0.503$ [24]). When $NPrSc^{-1} \gg 1$, the points are located on a straight line with a slope 1/4, in agreement with the result of the scale analysis. The cross-over between these two domains of variations, around $NPrSc^{-1} = 1$, is fairly narrow. In Fig. 6a, we have also reported numerical results obtained for $Sc = Pr$, i.e. when the asymptotic limit $Sc \gg Pr$ is not satisfied (full symbols). We note that the scaling established on the basis of $Pr \ll Sc$ still holds when $NPrSc^{-1} \ll 1$; this comes from the fact that heat transfer is governed by thermal convection so that it does not depend on the relative efficiency of heat and mass diffusion. When $NPrSc^{-1} \gg 1$, the points obtained for $Sc = Pr$ fall on a straight line which is parallel, but not superimposed on the line obtained for $Sc \gg Pr$. In this case, solutal convection dictates the velocity field and the heat transfer so that distinct prefactors are found depending on the relative importance of heat and mass diffusion.

Figure 6b is a log–log representation of the variations of $|\gamma'(0)|Pr^{1/3}Sc^{-1/3}$ as a function of $NPr^{1/3}Sc^{-1/3}$. Using this set of coordinates, all the points fall on a universal curve when the ratio $Sc/Pr$ is large enough (empty symbols). When $NPr^{1/3}Sc^{-1/3} \ll 1$, the chemical species transfer is governed entirely by thermal convection and $|\gamma'(0)|Pr^{1/3}Sc^{-1/3}$ is constant. When $NPr^{1/3}Sc^{-1/3} \gg 1$, the points are located on a straight line with a slope 1/4, in agreement with the result of the scale analysis. It is worth noting that the results for $Sc = 1000$ are very close to those expected in the asymptotic limit $N = \infty$, $Sc = \infty$ ($|\gamma'(0)| = 0.503$ when $N = \infty$, $Sc = \infty$, from ref. [9], p. 53). We have also reported data obtained for $Pr = Sc$ (full dots). They follow the scaling established in the limit $Pr \ll Sc$, but the values of the prefactors deserve some attention.

Indeed, when mass transfer is ruled by thermal convection ($NPr^{1/3}Sc^{-1/3} \ll 1$), the coupling between solutal and thermal effects yields different prefactors for $Sc = Pr$ and $Sc \gg Pr$. On the contrary, when mass transfer depends only on solutal effects ($NPr^{1/3}Sc^{-1/3} \gg 1$), the prefactors for $Pr = Sc$ and $Pr \ll Sc$ are very close.

The numerical results obtained for $Pr \ll 1 \ll Sc$ are reported in Fig. 7. They are also in agreement with the predictions of the scale analysis, and the same comments as previously given can be made concerning the position of the cross-overs, the scaling variations, and the existence and the values of the prefactors which compare quite well with the limits obtained in single-diffusive convection. Figure 7a is a log–log plot of $|\theta'(0)|Pr^{-1/4}$ vs $NPr^2Sc^{-1}$. Heat transfer switches from heat transfer ruled by thermal convection to heat transfer by mass convection around $NPr^2Sc^{-1} = 1$. Below the cross-over, the heat transfer scales as in pure thermal convection, just as predicted. The data calculated for $Pr = 10^{-3}$ are close to the asymptotic limit $|\theta'(0)|Pr^{-1/4} = 0.600$ obtained for $N = 0$ and $Pr = 0$ (ref. [9], p. 53); we also checked that the data calculated for $Pr = 0.1$, $Pr = 0.01$ coincide with the values found in pure thermal convection, i.e. they do not depend on the Schmidt number. Above the cross-over, the points fall on a straight line with a slope 1/4 as predicted. Figure 7b represents the variations of $|\gamma'(0)|Pr^{1/4}Sc^{-1/3}$ as a function of $NSc^{-1/3}$ in double-logarithmic coordinates. The agreement with the predictions reported in Table 3 is very good. We have

also reported data which are obtained for $Sc = 1$, i.e. outside the domain of validity for our predictions (full dots). The points form a curve which is parallel to the variations found for $Sc \gg 1$; it is worth noting that for $NSc^{-1/3} > 1$, the data are in excellent agreement with pure solutal convection at $Sc = 1$ and, again, they do not depend on the Prandtl number.

## 6. CONCLUDING REMARKS

Through the combined use of scale analysis and integral equations, the method developed here reveals new and meaningful features of double-diffusive convection. Our analysis makes it possible to derive systematically the different asymptotic flow configurations occurring in the vicinity of a vertical side wall in the presence of horizontal temperature and concentration gradients. Some of these flow configurations refer to degenerate situations in the sense that only two length scales are involved, exactly as in single-diffusive convection, but in general scale analysis relies on at least three length scales.

Some of the results presented in this work were already known from past literature, in particular those concerning the mass transfer coefficients at the wall [19–21]. They have been recovered easily by our analysis, their domain of validity has been assessed with precision and they have been completed by additional results concerning the temperature and velocity distributions. In addition, we have predicted several new behaviours which had never been considered before and we have got exhaustive predictions of the velocity, temperature and concentrations fields as a function of buoyancy forces and diffusivities. Each solution is characterized by several scaling relations involving a set of length and velocity scales following from $x[Ra_T(x)]^{-1/4}$ and $\alpha[Ra_T(x)]^{1/2}/x$ through factors depending on $N$, $Pr$ and $Sc$. These solutions are valid for asymptotically large or small $N$, $Pr$ and $Sc$ values, but our numerical study shows that the cross-overs between the different flows are fairly narrow, thus making our predictions suitable for practical purposes. Our most striking result deals with the existence of flows which are driven entirely by the temperature field, even though solutal forces are much greater than thermal forces.

At this point, it would be interesting to compare our predictions with experimental investigations. Unfortunately, only few experimental results can be found in the literature. Those available have focused on the measurements of mass transfer coefficients and concern only flows of type 2 [5, 6]; the data fit our prediction quite well. In view of this, we think that carefully designed experiments or numerical simulations covering a wide range of Prandtl and Schmidt numbers would be useful in the near future. Finally, although our method is simplified in comparison with real flows, its advantage is that it can be treated analytically, and we hope that it provides new insight that might be useful in interpreting double-diffusive convection in more complex geometries.

*Acknowledgements*—"Laboratoire Fluides, Automatique et Systèmes Thermiques" is a laboratory of Université Paris VI and is associated with CNRS (URA 871). One of us (AM) thanks the "Ecole Nationale des Ponts et Chaussées" for a grant.

## REFERENCES

1. J. S. Turner, *Buoyancy Effects in Fluids*. Cambridge University Press, Cambridge (1973).
2. W. A. Tiller, *The Science of Crystallization: Macroscopic Phenomena and Defect Generation*. Cambridge University Press, Cambridge (1991).
3. J. S. Turner, *A. Rev. Fluid Mech.* **17,** 11–44 (1985).
4. S. Ostrach, Natural convection with combined driving forces, *PhysicoChem. Hydrodyn.* **1,** 233–247 (1980).
5. J. A. De Leeuw den Bouten, B. de Mennik and P. M. Heertjes, Simultaneous heat and mass transfer in laminar free convection from a vertical plate, *Chem. Engng Sci.* **23,** 1185–1190 (1968).
6. Y. Kamotani, L. W. Wang, S. Ostrach and H. D. Jiang, Experimental study of natural convection in shallow enclosures with horizontal temperature and concentration gradients, *Int. J. Heat Mass Transfer* **28,** 165–173 (1985).
7. H. D. Jiang, S. Ostrach and Y. Kamotani, Thermosolutal convection flow regimes with opposed buoyancy forces in shallow enclosures, *PhysicoChem. Hydrodyn.* **10,** 599–613 (1988).
8. J. Lee, M. T. Hyun and K. W. Kim, Natural convection in confined fluids with combined horizontal temperature and concentration gradients, *Int. J. Heat Mass Transfer* **31,** 1969–1977 (1988).
9. B. Gebhart, Y. Jaluria, R. L. Mahajan and B. Sammakia, *Buoyancy-induced Flows and Transport*, Chap. 6. Hemisphere, Washington (1971).
10. H. Schlichting, *Boundary Layer Theory*. McGraw-Hill, New York (1968).
11. W. N. Gill, E. Del Casal and D. W. Zech, Binary diffusion and heat transfer in laminar free convection boundary layers on a vertical plate, *Int. J. Heat Mass Transfer* **8,** 1135–1151 (1965).
12. B. Gebhart and L. Pera, The nature of vertical natural convection flows resulting from the combined buoyancy effects of thermal and mass diffusion, *Int. J. Heat Mass Transfer* **14,** 2025–2050 (1971).
13. J. Srinivasan and D. Angirasa, Numerical study of double-diffusive free convection from a vertical surface, *Int. J. Heat Mass Transfer* **31,** 2033–2038 (1988).
14. R. L. Mahajan and D. Angisaran, Combined heat and mass transfer by natural convection with opposing buoyancies, *J. Heat Transfer* **115,** 606–612 (1993).
15. E. V. Somers, Theoretical considerations of combined thermal and mass transfer from a vertical plate, *J. Appl. Mech.* **23,** 295–301 (1956).
16. W. R. Wilcox, Simultaneous heat and mass transfer in free convection, *Chem. Engng Sci.* **13,** 113–119 (1961).
17. E. N. Lightfoot, Free-convection heat and mass transfer: the limiting case of $Gr_{AB}/Gr \to 0$ and $Pr/Sc \to 0$, *Chem. Engng Sci.* **23,** 931 (1968).
18. D. A. Saville and S. W. Churchill, Simultaneous heat and mass transfer in free convection boundary layers, *AICHE J.* **16,** 268–273 (1970).
19. A. Bejan, *Convection Heat Transfer*, Chap. 9. Wiley, New York (1993).
20. A. Bejan, *Solution Manual for Convection Heat Transfer*, pp. 172–177. Wiley, New York (1993).
21. K. R. Khair and A. Bejan, Mass transfer to natural

convection boundary layer flow driven by heat transfer, *J. Heat Transfer* **107,** 979–981 (1985).
22. O. V. Trenisan and A. Bejan, Combined heat and mass transfer by natural convection in a vertical enclosure, *J. Heat Transfer* **109,** 104–111 (1987).
23. C. Allain, M. Cloitre and A. Mongruel, Scaling in flows driven by heat and mass convection in a porous medium, *Europhys. Lett.* **20,** 313–318 (1992).
24. W. H. Press, B. P. Flannery, S. A. Teukolsky and W. T. Vetterling, *Numerical Recipes*, Chap. 11. Cambridge University Press, Cambridge (1986).

## APPENDIX

*Derivation of equations* (4)

Let us first express momentum conservation in sublayers $[0, \delta_T]$ and $[\delta_C, \delta_T]$ using relation (2a). The velocity derivatives in 0, $\delta_C$ and $\delta_T$ are: $(\partial u/\partial y)_0 \approx U_C/\delta_C$, $(\partial u/\partial y)_{\delta_C} \approx (U_T - U_C)/(\delta_T - \delta_C)$ and $(\partial u/\partial y)_{\delta_T} = 0$. The integrals of thermal buoyancy in $[0, \delta_T]$ and $[\delta_C, \delta_T]$ scale as $g\beta_T \Delta T \delta_1$ and $g\beta_T \Delta T(\delta_1 - \delta_C)$, respectively; the integral of solutal buoyancy between 0 and $\delta_C$ varies as $g\beta_C \Delta C N \delta_C$. In layers $[0, \delta_T]$ and $[\delta_C, \delta_T]$, advection is negligible so that the left-hand-side of equation (2a) can be set to zero. Finally, we obtain

$$0 \approx -\nu \frac{U_C}{\delta_C} + g\beta_T \Delta T(\delta_T + N\delta_C) \tag{A1}$$

$$0 \approx -\nu \frac{U_T - U_C}{\delta_T - \delta_C} + g\beta_T \Delta T(\delta_1 - \delta_C). \tag{A2}$$

Equation (A1) gives directly equation (4a). After substituting $U_C$ by its expression (4a) into (A2) and keeping the leading terms ($\delta_C \ll \delta_T$), we find equation (4b). It is worth noting that relation (A1) cannot be obtained from the local conservation equations (1), because $u$ has two different scales in $[0, \delta_C]$ and in $[\delta_C, \delta_T]$. On the contrary, equation (A2) can be derived from the local equations (1), because $u$ varies uniformly in $[\delta_C, \delta_T]$.

Heat conservation in $[0, \delta_1]$ and chemical species conservation in $[0, \delta_C]$ are expressed using relations (2b) and (2c), which read

$$\frac{U_C}{x}\delta_C + \frac{U_1}{x}(\delta_1 - \delta_C) \approx \alpha \frac{1}{\delta_1} \tag{A3}$$

$$\frac{U_C}{x}\delta_C \approx D\frac{1}{\delta_C}. \tag{A4}$$

Since $U_T \geqslant U_C$ and $\delta_C \ll \delta_T$, (A3) reduces to equation (4c). Equation (A4) gives directly equation (4d).

Relations (A1)–(A4) make it possible to find $U_C$, $U_T$, $\delta_C$ and $\delta_T$, but an additional relation is necessary for determining $\delta$. We express that the flow in $[\delta_T, \delta]$ is ruled by a balance between inertia and friction, using the local equation (1a), and we get

$$\frac{U_T^2}{x} \approx \nu \frac{U_T}{\delta^2}. \tag{A5}$$

This equation is equivalent to (4e).

*Derivation of equations* (5)

To establish equations (5), we express momentum conservation in sublayers $[0, \delta_v]$, $[\delta_C, \delta_v]$ and $[\delta_v, \delta_T]$ using relation (2a), heat conservation in $[0, \delta_T]$ using equation (2b), and chemical species conservation in $[0, \delta_C]$ using equation (2c). These different relations read

$$0 \approx -\nu \frac{U_C}{\delta_C} + g\beta_T \Delta T(\delta_v + N\delta_C) \tag{A'1}$$

$$0 \approx -\nu \frac{U_v - U_C}{\delta_v - \delta_C} + g\beta_1 \Delta T(\delta_v - \delta_C) \tag{A'2}$$

$$\frac{U_v^2}{x}(\delta_T - \delta_v) - U_v V_v \approx g\beta_T \Delta T(\delta_T - \delta_v) \tag{A'3}$$

$$\frac{U_C}{x}\delta_C + \frac{U_v}{x}(\delta_1 - \delta_C) \approx \alpha \frac{1}{\delta_T} \tag{A'4}$$

$$\frac{U_C}{x}\delta_C \approx D\frac{1}{\delta_C}. \tag{A'5}$$

Equations (A'1) and (A'5) give directly equations (5a) and (5e). Equation (A'2) reduces to equation (5b) since $\delta_C \ll \delta_v$, and (A'4) to equation (5d) since $\delta_C \ll \delta_T$ and $U_C \leqslant U_v$. Owing to incompressibility, we have: $V_v \approx U_v \delta_v / x$; substituting into (A'3) and keeping only the leading terms ($\delta_T \gg \delta_v$), leads to relation (5c).

*Derivation of equations* (5′)

We apply equation (2a) to layers $[0, \delta_C]$ and $[\delta_v, \delta]$, equation (2b) to $[0, \delta_T]$ and equation (2c) to $[0, \delta_C]$

$$0 \approx -\nu \frac{U_C}{\delta_C} + g\beta_T \Delta T(1 + N)\delta_C \tag{A''1}$$

$$\frac{U_v^2}{x}(\delta_T - \delta_v) - U_v V_v \approx g\beta_T \Delta T(\delta_T - \delta_v) \tag{A''2}$$

$$\frac{U_C}{x}\delta_v + \frac{U_v}{x}\delta_T \approx \alpha \frac{1}{\delta_T} \tag{A''3}$$

$$\frac{U_C}{x}\delta_C \approx D\frac{1}{\delta_C}. \tag{A''4}$$

Equations (A″1), (A″3) and (A″4) give directly equations (5′a), (5′c) and (5′d). From incompressibility, we deduce that: $V_v \approx U_v \delta_v / x$; substituting into equation (A″2) and using the inequality $\delta_T \ll \delta_v$, expression (A″2) simplifies into equation (5′b). Finally, the balance between friction and inertia in layer $[\delta_C, \delta_v]$ dictates that

$$\frac{U_C^2}{x} \approx \nu \frac{U_C}{(\delta_v - \delta_C)^2}. \tag{A''5}$$

Since $\delta_C \ll \delta_v$, equation (A″5) gives equation (5′e).